

SERSbot: Revealing the details of SERS multi-analyte sensing using full automation

David-Benjamin Grys¹, Bart de Nijs¹, Junyang Huang¹, Oren A Scherman,² Jeremy J. Baumberg^{1*}

¹ NanoPhotonics Centre, Cavendish Laboratory, Department of Physics, JJ Thompson Avenue, University of Cambridge, Cambridge, CB3 0HE, United Kingdom

² Melville Laboratory for Polymer Synthesis, Department of Chemistry, University of Cambridge, Lensfield Road, Cambridge CB2 1EW, UK

*email: jjb12@cam.ac.uk

Table of contents

Photos of SERSbot components (Figure S1)
AuNP aggregation by MV (Figure S2)
CB[7]:MV²⁺/d₈-MV²⁺ DFT and thermochemistry (Figure S3, Table S1)
Robot raw spectra (Figure S4)
CB[5] versus CB[7] and MV²⁺ in the nanogap (Figure S5)
Langmuir-Hill fit calculations
Model comparison (Figure S6, Table S2)
ICA Matlab code
Video Caption (Video S1)
References

Photos of SERSbot components

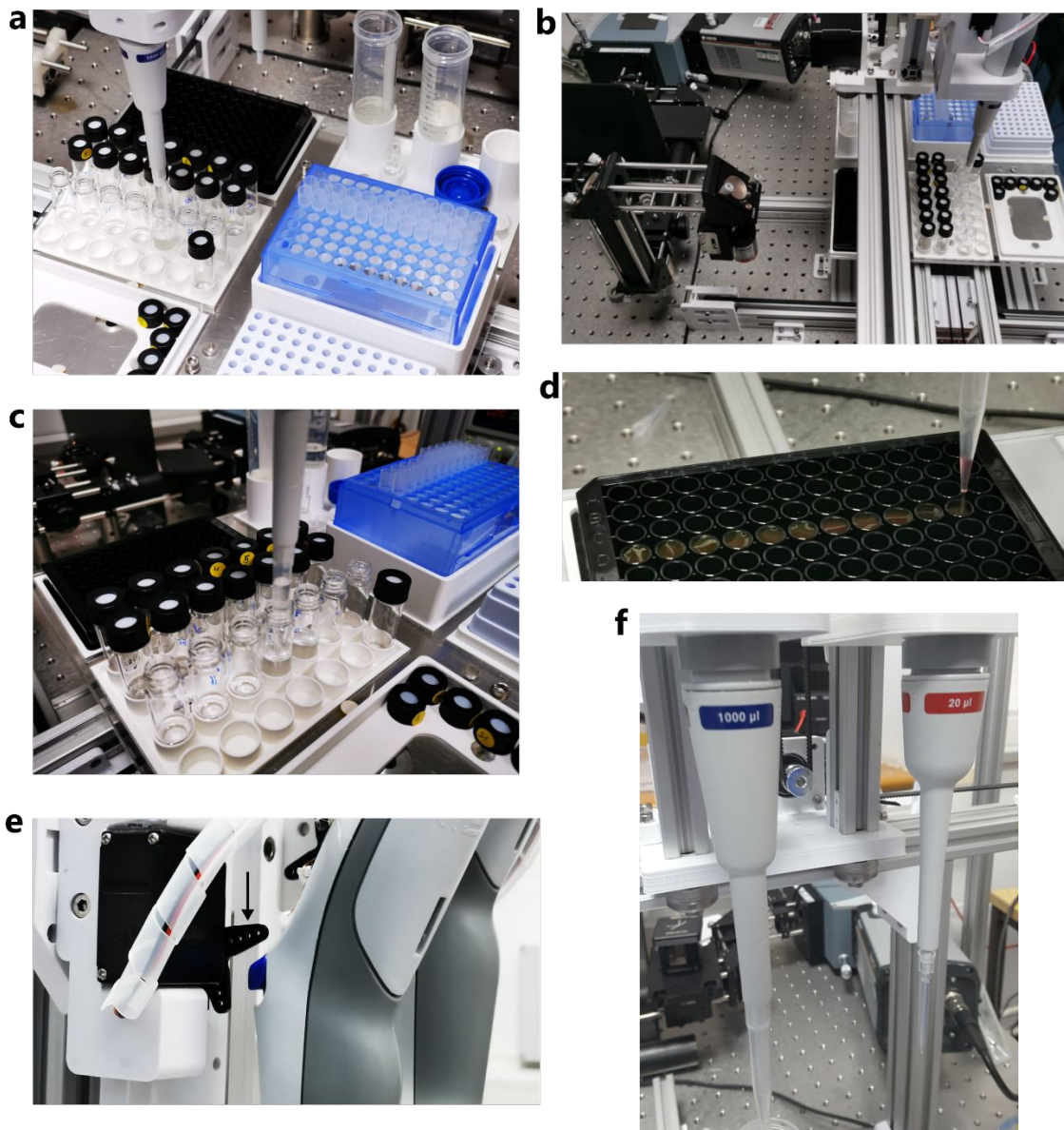


Figure S1 SERSbot photographs. (a) Platform with various vials, tip containers. (b) Raman setup with objective attached to liquid handler. (c) Pipette, dispensing liquid into glass vial. (d) AuNP dispensing into multiwell plate. (e) Servo triggering the pipette eject button (direction of black arrow). (f) Two electric pipettes 50-1000 μ L and 0.5-20 μ L used by the SERSbot.

AuNP aggregation by MV

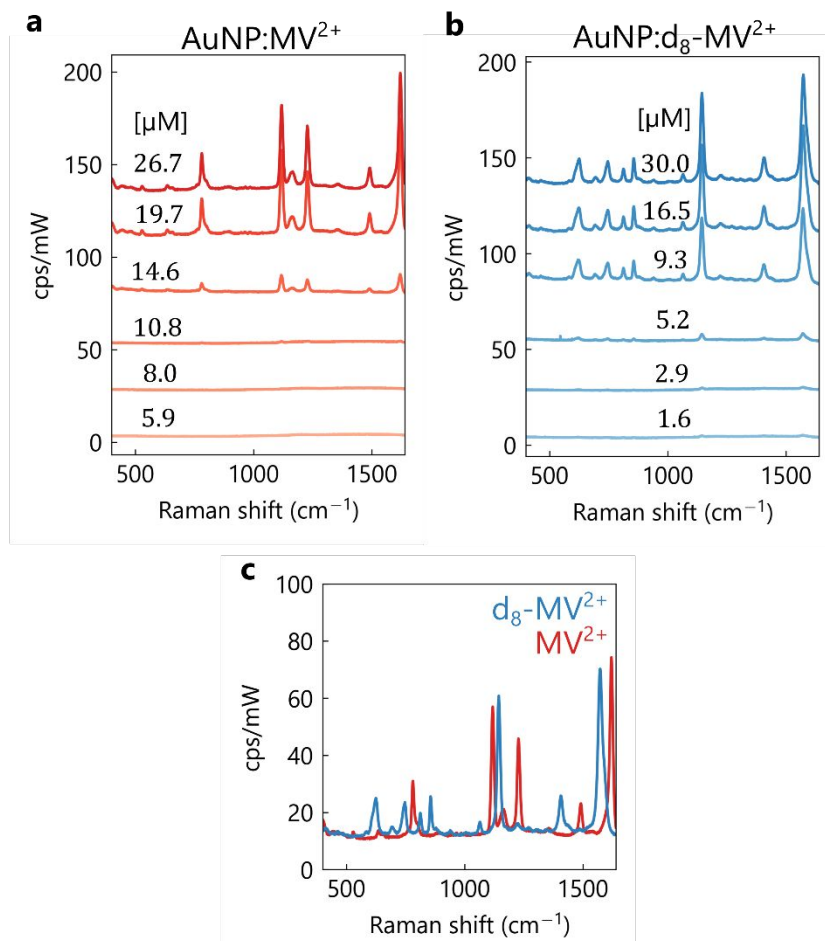


Figure S2 AuNP aggregation by MV. (a,b) Concentration series of (a) MV²⁺ and (b) d₈-MV²⁺ mixed into AuNPs demonstrating aggregation of AuNPs for high concentrations. Here 20 μL of (d₈-)MV²⁺ is mixed with 320 μL of AuNPs. The aggregation time is fixed to 60 s. (c) Direct comparison of MV²⁺ and d₈-MV²⁺.

CB[7]:MV²⁺/d₈-MV²⁺ DFT and thermochemistry

The optimised geometries of CB[7] complexes with MV²⁺ and d₈-MV²⁺ are shown in Figure S3(a,b). CB[7] forms an almost identical 1:1 inclusion complex with the regular and perdeuterated MV²⁺. Therefore, the complexation energy, enthalpy, and Gibbs free energy (Table S1) are also nearly identical. The slightly greater molecular weight (~8 m.u.) however, has a significant influence on the vibrational spectrum as seen in the measurement (main text) and predicted by DFT calculations (Figure S3c).

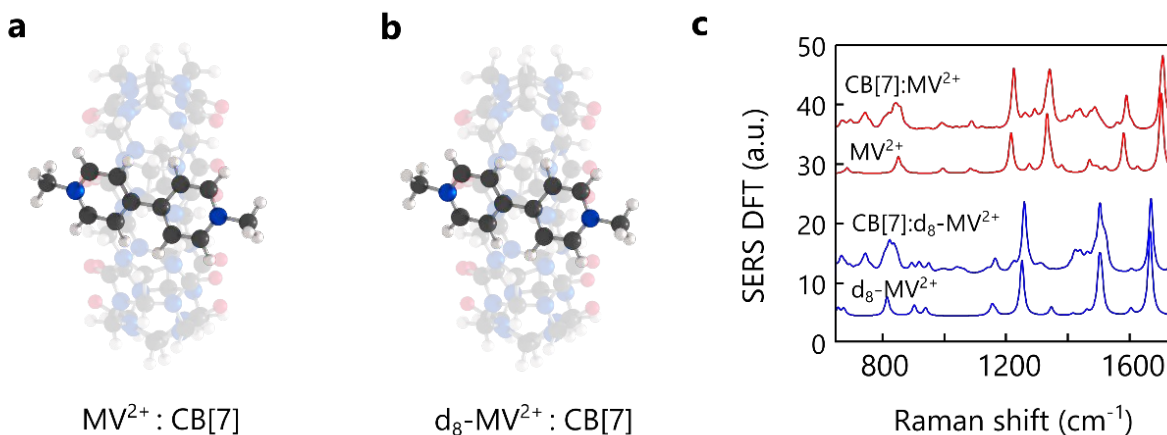


Figure S3 DFT calculation. (a,b) optimised geometries for the 1:1 inclusion complex of CB[7] with MV^{2+} and d_8-MV^{2+} . (c) Comparison of DFT calculated vibrational spectrum between MV^{2+}/d_8-MV^{2+} and their CB[7] inclusion complex.

Furthermore, it is interesting to observe that the inclusion complex vibrational spectrum contains peak shifts due to the hydrophobic CB[7] cavity and interactions of the positively charged nitrogen with the carbonyl oxygens at the CB[7] portals.

The thermochemistry calculations (Table S1) are counterpoise corrected to compensate for the basis set super position error when using the limited 6-31G*/GD3BJ basis set. The rigid-rotor-harmonic-oscillator (RRHO) approximations for entropy and enthalpy are corrected by the quasi-harmonic approximation. For the vibrational entropy a 100 cm^{-1} cut-off is employed. The calculations are performed using 'goodvibes'.¹

CB[7] complex	$\Delta E(SMD)$	E_{BSSE}	$\Delta H(SMD)$	$\Delta G(SMD)$
d_8-MV^{2+}	-51.4584	13.64	-35.7	-18.9
MV^{2+}	-51.4584	13.64	-35.6	-18.8

Table S1 Thermochemistry calculations. Complexation energy, basis set superposition error (counterpoise) energy correction, enthalpy and Gibbs free energy. All values provided are in kcal/mol units.

Robot raw spectra

Typical raw spectra, before applying independent component analysis, recorded by the SERSbot are shown in Figure S4 a-c.

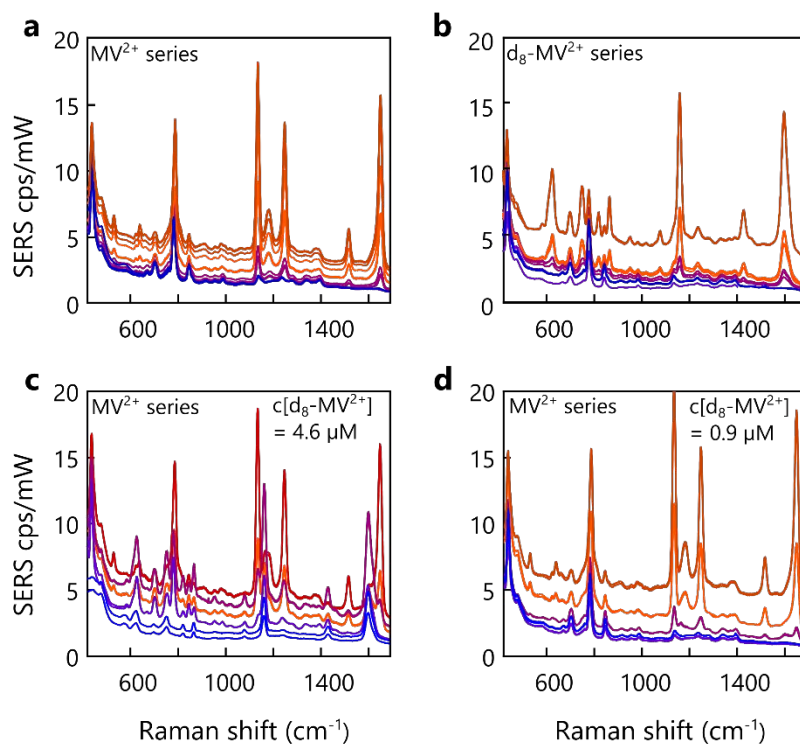


Figure S4 MV²⁺/d₈-MV²⁺ concentration series. (a) Raw data of CB[7]:AuNP aggregates for MV²⁺ concentration series. (b) Same, but d₈-MV²⁺ is varied. (c) d₈-MV²⁺ concentration fixed to 4.7 μM, MV²⁺ varied. (d) d₈-MV²⁺ concentration fixed to 0.9 μM, and MV²⁺ varied.

CB[5] versus CB[7] and MV²⁺ in the nanogap

It is well known that MV²⁺ is sequestered in solution by CB[7] molecules outside the nanogap forming a 1:1 inclusion complex.² The cavity of the homologue CB[5] is too small to sequester MV²⁺. In our measurements however, we see that strong MV²⁺ signals are produced by both CB[5] and CB[7] AuNP aggregates (Figure S5). This leads to the conclusion that MV²⁺ is not sequestered by CB[7] molecules inside the nanogap, and the CB[n] molecules are solely acting as molecular spacers.³ This is also evident from the direct comparison of the dominant MV²⁺ peaks in CB[5] and CB[7] aggregates; sequestered MV²⁺ inside the hydrophobic cavity would produce peak shifts between CB[5] and CB[7] aggregates as clearly seen in the DFT calculations for free and CB[n]-bound MV²⁺.

However, in the measurements the MV^{2+} peaks almost perfectly align (Figure S5, black arrows).

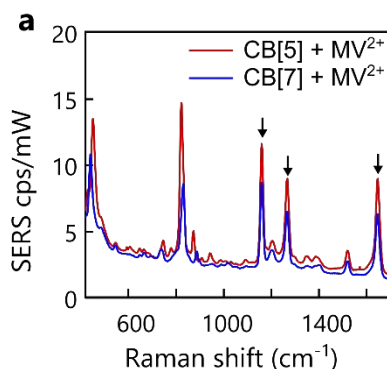


Figure S5 CB[5]/CB[7] comparison. (a) Comparison of MV^{2+} spectra in CB[5] (red) and CB[7] AuNP aggregates. Black arrow shows dominant MV^{2+} vibrations.

Langmuir-Hill fit

To extract the disassociation constant from a ligand concentration series, we use a standard Langmuir-Hill fit.⁴ The disassociation constant K_d is defined as the ratio of the product between unbound ligand [L] and receptor [R] to the total concentration of complexes [L · G]

$$K_d = \frac{[L][R]}{[L \cdot R]}$$

By solving this equation for the receptor concentration [R] and substituting it into the mass conservation equation

$$[R_0] = [R] + [L \cdot R]$$

with $[R_0]$ denoting the total number of receptors, we arrive at the Langmuir-Hill equation

$$\frac{[L \cdot R]}{[R_0]} = \frac{1}{1 + \frac{K_d}{[L]}}$$

setting the Hill coefficient n to unity with $K_d = (K_{HO})^n$. Here, K_{HO} corresponds to the ligand concentration occupying half of the receptors.

Model comparison

Figure S6 shows the model response to the measured dissociation constants (see main text section "Competitive binding assay"). As can be seen, the peak resonance effect at 1 μM is not correctly modelled without a (geometric) AuNP surface area correction (Figure S6 a,b). The model parameters used are summarised in Table S2.

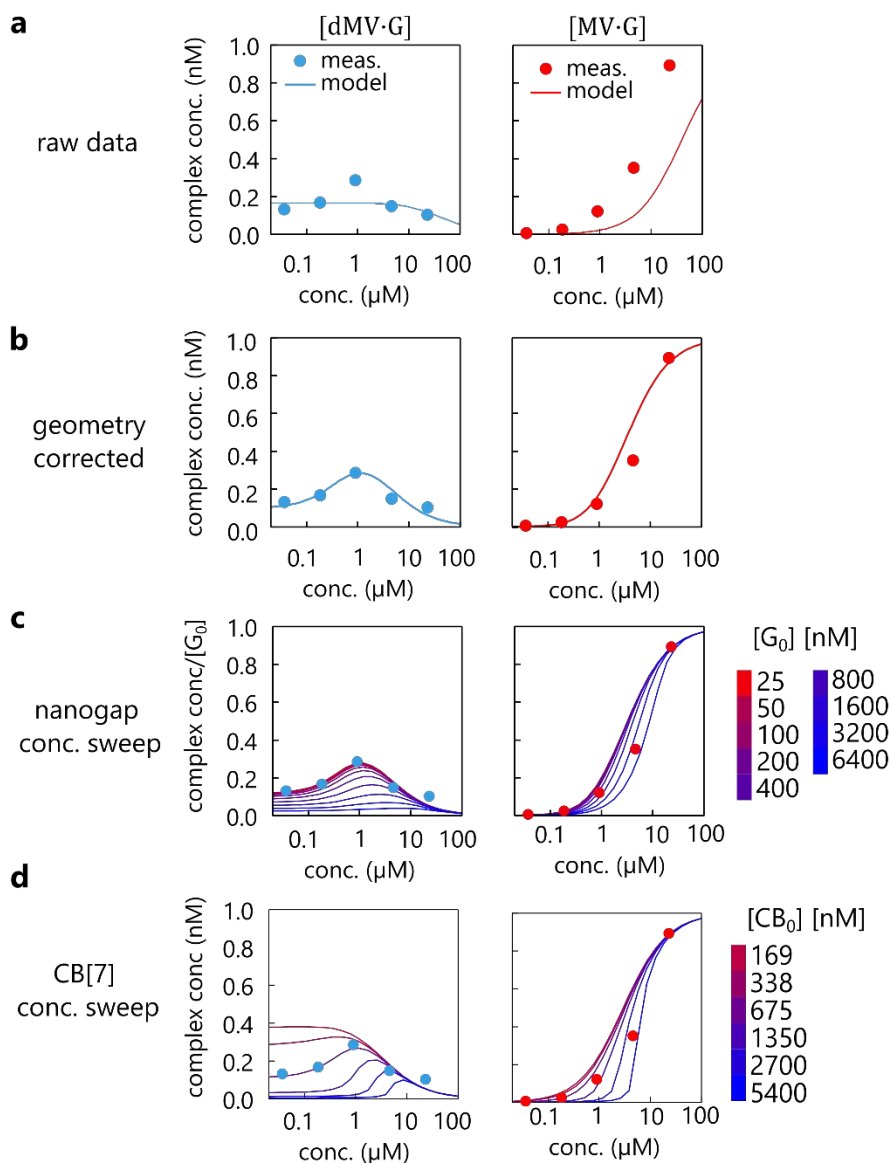


Figure S6 model calculations. (a) Calculations performed and matched with measured raw data. (b) Geometry corrected calculations to give corrected d-MV/MV concentrations and higher

binding affinity. (c) Parametrised gap concentration sweep, and (d) sweep over CB[7] concentration.

Fig	model	$K_d^{G:MV}$	$K_d^{G:dMV}$	$K_d^{CB:(d)MV}$	$[G_0]$	$[CB_0]$	$[dMV_0]$	$[MV_0]$
(a)	measured	20 μ M	32 μ M	0.1 μ M	100 nM	0.68 μ M	4.6 μ M	variable
(b)	corrected	0.63 μ M	1.5 μ M	0.3 μ M	100 nM	0.68 μ M	4.6 μ M	variable
(c)	vary gap	0.63 μ M	1.5 μ M	0.3 μ M	param	0.68 μ M	4.6 μ M	variable
(d)	vary CB[7]	0.63 μ M	1.5 μ M	0.3 μ M	100 nM	param	4.6 μ M	variable

Table S2 model parameter. Summary of model parameters used for plots in Figure S6.

ICA Matlab code⁵

```

%% ICA demonstration for SERS spectra
%based on Hyvarinen "Fast and robust fixed-point algorithms for
%independent component analysis", IEEE transactions on Neural
%Networks, 1995

    clc
    clear

%% input data
    load('MV-DMV-60.mat')
    X = waves'; % 60x1600 matrix 'waves', 60 spectra, 1600 pixels(CCD)

%% removing mean from data
    mu_X = mean(X'); % calculating mean
    M = repmat(mu_X',1,length(X)); % mean matrix
    mX = X-M; % subtracting mean

%% data whitening/PCA
    cov_X = cov(mX'); % calculating covariance
    [E,D] = eig(cov_X); % calculating eigenvectors/values

    D2 = real(diag(diag(D.^(-1/2)))); % whitening

    V = D2*E';
    v = V*mX; % sum(diag(cov(v')) = 60
    v = v(58:end,:); % pick three most significant PCA spectra

%% ICA algorithm
    n = length(v(:,1));
    B = zeros(n);
    for(r = 1:n)
        w0 = rand(n,1);
        w1 = rand(n,1);

        if (r > 1)
            w0 = w0-B*B'*w0; % "removing" found component

```

```

end

w0 = w0/norm(w0);

eps = 1e-12;
for(i = 1:1000) %% limit to 1000 iterations

    w1 = (v*((v'*w0).^4))/1-3*w0; % ICA gradient descent
    w1 = w1/norm(w1);

    if (norm(w0-w1) < eps) % convergence criterion
        break
    end

    w0 = w1;
end

B(:,r) = w0; % store ICA component
end

%% Plotting components
p = B'*v*1;
for z=1:n
    plot(1:1600,p(z,:)+z*10) % plotting with offset
    hold on
end
hold off
%% End of code

```

Video caption

Video S1 SERSbot pipette tip change. Automated tip attachment and release is demonstrated for 100 pipette tips in real speed (first tip) and sped up for the following 99 tips.

REFERENCES

- (1) Luchini, G.; Alegre-Requena, J. V.; Funes-Ardoiz, I.; Paton, R. S. GoodVibes: Automated Thermochemistry for Heterogeneous Computational Chemistry Data. *F1000Research* **2020**, *9*, 291.
- (2) Ong, W.; Kaifer, A. E. Salt Effects on the Apparent Stability of the Cucurbit[7]Uril-Methyl Viologen Inclusion Complex. *J. Org. Chem.* **2004**, *69* (4), 1383–1385.
- (3) De Nijs, B.; Carnegie, C.; Szabó, I.; Gryś, D.-B.; Chikkaraddy, R.; Kamp, M.; Barrow, S. J.; Readman, C. A.; Kleemann, M.-E.; Scherman, O. A.; Rosta, E.; Baumberg, J. J. Inhibiting Analyte Theft in Surface-Enhanced Raman Spectroscopy Substrates: Subnanomolar Quantitative Drug Detection. *ACS Sensors* **2019**, *4* (11).
- (4) Weiss, J. N. The Hill Equation Revisited: Uses and Misuses. *FASEB J.* **1997**.
- (5) Hyvärinen, A. Fast and Robust Fixed-Point Algorithms for Independent Component Analysis. *IEEE Trans. Neural Networks* **1999**, *10* (3), 626–634.